ISPRS Journal of Photogrammetry and Remote Sensing 95 (2014) 13–22

Contents lists available at ScienceDirect

ISPRS Journal of Photogrammetry and Remote Sensing

journal homepage: www.elsevier.com/locate/isprsjprs

Remote spectral imaging with simultaneous extraction of 3D topography for historical wall paintings

Haida Liang [a,*], Andrei Lucian [a], Rebecca Lange [a], Chi Shing Cheung [a], Bomin Su [b]

[a] School of Science and Technology, Nottingham Trent University, Nottingham NG11 8NS, UK
[b] Conservation Research Institute, Dunhuang Academy, Gansu Province 736200, China

ARTICLE INFO

Article history:
Received 22 January 2014
Received in revised form 22 May 2014
Accepted 23 May 2014

Keywords:
Cultural heritage
Archaeology
Hyper spectral
Metrology
Multispectral
Three-dimensional

ABSTRACT

PRISMS (Portable Remote Imaging System for Multispectral Scanning) is designed for in situ, simultaneous high resolution spectral and 3D topographic imaging of wall paintings and other large surfaces. In particular, it can image at transverse resolutions of tens of microns remotely from distances of tens of metres, making high resolution imaging possible from a fixed position on the ground for areas at heights that is difficult to access. The spectral imaging system is fully automated giving 3D topographic mapping at millimetre accuracy as a by-product of the image focusing process. PRISMS is the first imaging device capable of both 3D mapping and spectral imaging simultaneously without additional distance measuring devices. Examples from applications of PRISMS to wall paintings at a UNESCO site in the Gobi desert are presented to demonstrate the potential of the instrument for large scale 3D spectral imaging, revealing faded writing and material identification.

1. Introduction

Spectral imaging (i.e. multispectral and hyperspectral imaging) was first developed for remote sensing and astronomy (Goetz et al., 1985). It is an efficient method of collecting spectral reflectance at millions of points. By the 1990s, multispectral imaging (less than 10 spectral bands) was applied to imaging of old master paintings in museums and galleries (Derrien et al., 1993; Martinez et al., 1993). Initially it was used to improve colour accuracy of the images captured and for qualitative comparison between the bands. Later, spectral imaging was used to obtain reflectance spectra for pigment identification (Baronti et al., 1998; Casini et al., 1999; Liang et al., 2005). Other applications of spectral imaging in art include imaging of underdrawings beneath the paint layers. Most paints are more transparent in the near infrared and hence images in the infrared are useful for revealing the preparatory drawings beneath the paint (van Asperen de Boer, 1968; Liang et al., 2013). A comparison between images in the visible spectral range with those in the near infrared can also reveal past interventions and damages to the paintings, since conservators colour match the paint for retouching to the original without necessarily using the same paint material. Two materials that are colour matched do not necessarily have the same appearance in the near infrared. Comprehensive reviews on spectral imaging applications in art conservation and archaeology can be found in a number of reviews (Liang, 2012; Kubik, 2007; Fischer and Kakoulli, 2006).

Spectral imaging systems in museums are usually scanning devices used in close range (<2 m) from the paintings to obtain high resolution spectral images. In some cases, fixed mechanical scanners are built to move, either the imaging device or the painting, in order to scan an entire painting. The size of a painting that can be imaged will be limited by the scanner size and by the size of the studio for the very large movable paintings. Such imaging systems are not suitable for imaging paintings such as wall paintings and extremely large easel paintings, since these need to be imaged in situ. Free standing spectral imaging camera with a normal lens will not be able to image large paintings or paintings at lofty heights (e.g. ceiling paintings) at high resolution without scaffolding. For example, a mechanical elevator weighing nearly a tonne was built to bring a colour camera close to the target in a project to image stained glass panels in churches (Macdonald, 2006); scaffolding towers were built on tracks to use a colour camera to scan the wall paintings at Mogao caves in Dunhuang (Wallach, 2004). Apart from the complexity of using heavy and cumbersome mechanical structures, a major problem with these methods is that the images cannot be correctly mosaiced together because of parallax since each neighbouring image is captured with the camera at

* Corresponding author. Tel.: +44 1158488056.
E-mail address: Haida.Liang@ntu.ac.uk (H. Liang).

http://dx.doi.org/10.1016/j.isprsjprs.2014.05.011
0924-2716/

a different position. This is usually not a problem for very flat paintings such as easel paintings, but wall paintings by nature have significant 3D structure. In this paper, we present an imaging system that is capable of remote high resolution imaging from a fixed position on the ground by using a telescope on an alt-az mount that avoids parallax.

Historical wall paintings are often found in houses, churches, cathedrals, temples, caves and tombs. They are particularly vulnerable and difficult to image. Wall paintings can be visually represented by the spectral reflectance per pixel and the 3D spatial structure. Spectral imaging provides not only material identification but also the colour image under lighting of any emission spectra. Currently, 3D imaging of wall paintings are usually achieved by laser scanning or photogrammetry. To obtain simultaneous spectral reflectance and 3D topographic measurements, the 3D data will then have to be spatially registered with spectral imaging data (Brusco et al., 2006; Barazzetti et al., 2010). An alternative method is to acquire 3D texture information by using two cameras and in different wavelengths (Mara et al., 2009). Such methods of acquiring 3D multispectral imaging data needs two separate instruments for acquisition which increases both instrumental and post-processing complexity as well as the cost. In addition, none of the systems has so far been able to achieve remote imaging at transverse resolution better than 1mm at distances greater than a few metres.

In this paper, we demonstrate a spectral imaging system that allows automatic, in situ, remote imaging (distances up to 35 m) of paintings at high resolution that gives not only spectral information per pixel of the paintings, but also 3D position and distance measurements as a by-product. Applications of the remote imaging instrument to a UNESCO world heritage site, Mogao caves, along the Silk Road will be discussed.

2. PRISMS – Portable Remote Imaging System for Multispectral Scanning

PRISMS is designed for portable, flexible and versatile remote imaging, consisting of modular components: (1) for imaging at distances >3–4 m, a telescope (focal length 1250 mm and aperture diameter 90 mm) is used; (2) for close range imaging at distances <3–4 m, lenses are used; (3) for imaging in the range 400–900 nm (VIS/NIR), interference filters are used with CCD detectors (Liang et al., 2007); and (4) for imaging in the 900–1700 nm range (SWIR), an imaging AOTF spectrograph and an InGaAs detector are used (Liang et al., 2010). This paper will concentrate on 3D spectral imaging with the VIS/NIR multispectral imager, which is a simple, low budget instrument consisting of a filter wheel with 10 filters and a CCD camera. The first 9 filters are centred at 400–800 nm at 50 nm spacing and 40 nm bandwidth. The last filter is at 880 nm with 70 nm bandwidth. The modest spectral resolution is a trade-off with speed of capture. In general most natural material such as paint have rather smooth reflectance spectra and hence little loss in information by reducing the spectral resolution to 50 nm. Only a handful of pigments such as cobalt blue and some red lake pigments require spectral resolutions of 15 nm. Fig. 1 shows the system: the camera, filter wheel and telescope are placed on an alt-az mount that can be computer controlled. PRISMS is arranged in such a way that the telescope optical axis passes through the pivot of the two mechanical axes to avoid parallax.

Active illumination is used in the present application of close range remote imaging (within 35 m), unlike normal remote sensing where passive illumination from the Sun is used. A tungsten halogen light with an optical system that projects a flat illumination of 10° is used for remote illumination. For imaging at distances >5 m a 900 W tungsten bulb with colour temperature of 3200 K is used. The light is selected to give maximum illumination for fast capture without causing damage to the paintings. Temperature increase due to illumination was measured with a highly absorbing liquid crystal thermometer (i.e. worst case scenario similar to the effect on a black paint) at a distance of 10 m and found to be <2 °C (the accuracy of the thermometer is 2°) above ambient temperature of 22 °C for the light source using the 900 W bulb. The light is mounted on an identical alt-az mount as the telescope and the movements of the two mounts are synchronised. The light and the telescope system are placed as close as possible with the optical axis of the light at an angle of ~5° to the optical axis of the telescope such that the light will always illuminate the area imaged at all distances >3 m.

The spectral transmission of the filters and the overall spectral response of the system using the 900 W light are shown in Fig. 2.

3. System characteristics and remote calibration

Calibration of spectral imaging systems in a fixed laboratory setting is well established. It generally involves dark current subtract, flatfield calibration to correct for non-uniform illumination and pixel to pixel gain variation of the CCD sensor, and spectral calibration with a spectral standard such as a Labsphere Spectralon white target. In these cases the white standard is usually placed at exactly the same position and orientation as the imaging target.

Remote imaging presents a number of challenges since it is not practical to take an image of the white standard at each imaging position. In the following sections, we will discuss the methods used for remote calibration as well as the system characteristics.

3.1. Spatial resolution

A He–Ne laser with a 5 μm diameter fibre output was placed at 7 m from PRISMS as a point source to measure the Point Spread Function (PSF) of PRISMS in the configuration with the telescope using the 650 nm filter. The intensity of the laser was adjusted to a minimum so that the integration time was 1 ms. The FWHM PSF of the system was found to be ~ 1.7″ which corresponds to ~ 60 μm on the target at a distance of 7 m. The PSF thus measured is unlikely to be affected by lab 'seeing' (air turbulence) because of the short integration time. However, realistic integration times are likely to be in the range of tens of milliseconds to a few seconds depending on the distance, the filter and the target. The 'seeing' was measured by taking the standard deviation of the peak positions of the laser taken successively over a period of 25 s which provides the worst case scenario. The lab 'seeing' over a 25 s period was found to be 1.6″ FWHM measured at a distance of 4 m. Typical integration time of PRISMS is of the order of hundreds of milliseconds, therefore the effect of seeing is likely to be much less than 1.6″. However, these measurements are taken in a temperature regulated enclosed lab. When long distance measurements (>10 m) were performed in the corridor outside the lab, seeing effects were much more noticeable as will be discussed in the next section.

3.2. Metrology

In order to perform remote calibration and measure 3D surface topography, we need to measure the distance from the imaging system to the target position. In this section, we show that the spectral imaging system can determine the distance without extra measurements such as laser scanning.

Since it is always necessary to focus the image, the target distance can be determined by the position of focus. The unique

Fig. 1. (a) PRISMS: lighting system on an alt-az mount (top) and imaging system (bottom) with telescope, filter wheel and camera on another alt-az mount and (b) PRISMS at work imaging cave paintings at Mogao caves in the Gobi desert.

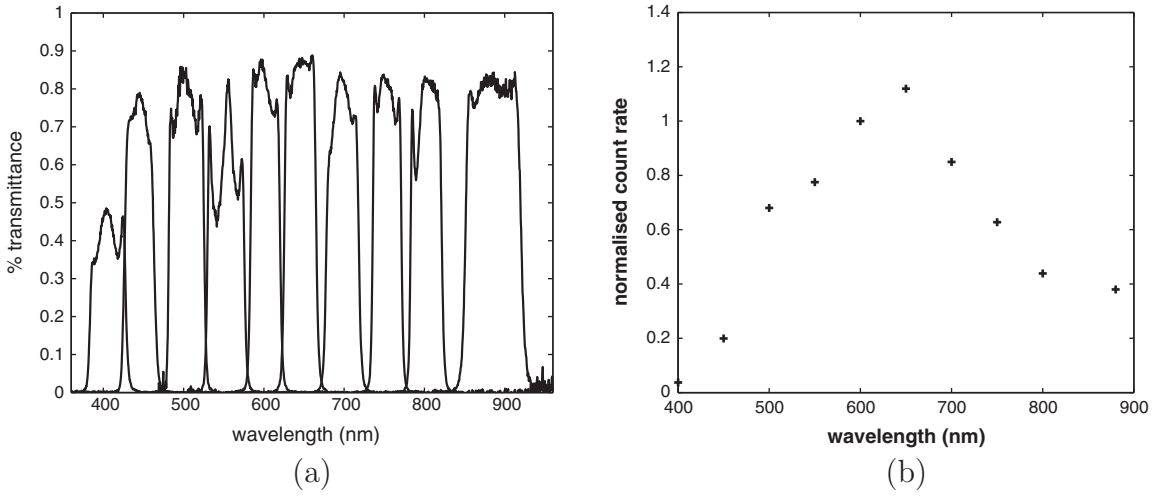

Fig. 2. (a) VIS/NIR filter transmission spectra and (b) overall spectral response of the system.

relation between the object distance and the image distance is given by the lens maker's formula. In PRISMS, an image quality metric is used to determine the sharpness of the image and hence the position of best focus. Focusing is done in the filter that is most efficient, that is at 650 nm (see Fig. 2b). The same focus position is adequate for all filters when using the telescope. The following five image quality metrics were tested:

1. Variance, defined by:

$$V = (M \times N)^{-1} \sum_x \sum_y [f(x,y) - \mu]^2, \tag{1}$$

where $f(x,y)$ is the grey level intensity of pixel (x,y) of a $M \times N$ image, and

$$\mu = \frac{1}{M \times N} \sum_x \sum_y f(x,y). \tag{2}$$

2. Energy of image gradient (EoG).

$$\mathrm{EoG} = \sum_x \sum_y (f_x^2 + f_y^2), \tag{3}$$

where $f_x = f(x+1,y) - f(x,y)$ and $f_y = f(x,y+1) - f(x,y)$.

3. Spatial frequency (SF).

$$\mathrm{SF} = \sqrt{\mathrm{RF}^2 + \mathrm{CF}^2} \tag{4}$$

where RF is the row frequency

$$\mathrm{RF} = \sqrt{\frac{1}{M \times N} \sum_{x=1}^{M} \sum_{y=2}^{N} [f(x,y) - f(x,y-1)]^2} \tag{5}$$

and CF the column frequency

$$\mathrm{CF} = \sqrt{\frac{1}{M \times N} \sum_{x=2}^{M} \sum_{y=1}^{N} [f(x,y) - f(x-1,y)]^2}. \tag{6}$$

4. Energy of the Laplacian of the image (EoL).

$$\mathrm{EoL} = \sum_x \sum_y f_{xy}^2 \tag{7}$$

where f_{xy} is a mask with coefficients $\begin{Bmatrix} -1 & -4 & -1 \\ -4 & 20 & -4 \\ -1 & -4 & -1 \end{Bmatrix}$ centred on pixel (x,y).

5. Sum-modified Laplacian (SML).

$$\mathrm{SML} = \sum_{i=x-N}^{x+N} \sum_{j=y-N}^{y+N} \nabla_{ML}^2 f(i,j) \quad \text{for } \nabla_{ML}^2 f(i,j) \geqslant T. \tag{8}$$

where

$$\begin{aligned} \nabla_{ML}^2 f(x,y) &= |2f(x,y) - f(x - \mathrm{step},y) - f(x + \mathrm{step},y)| \\ &\quad + |2f(x,y) - f(x,y - \mathrm{step}) - f(x,y + \mathrm{step})|. \end{aligned} \tag{9}$$

and where T is a threshold value and N sets the size of the window used to calculate the metric. The *step* parameter allows for different size of texture elements (Nayar and Nakagawa, 1994). In our experiments, we have only used a value of 1 for the *step*.

At high integration time, all the above metrics produce good results, however, for imaging efficiency we need the metric that works at lower integration times. The SML algorithm is generally found to be the best choice in both accuracy and implementation time (Huang and Jing, 2007). However, for low exposure times or low reflectivity targets, the EoG was the best option and it is also computationally the fastest.

For most surfaces we image a region of interest (ROI) $\frac{1}{4}$ the size of the entire image for focusing. It was found that an integration time 10% of the maximum exposure time without saturating the CCD detector was adequate for focusing. A higher integration time (50% of the maximum exposure time) is needed for darker areas with reflectance less than a few percent. Fig. 3a shows an example plot of EoG focus measure metric versus relative distance at around 7 m. The peak position of the Gaussian fit provides the best estimate of the focus position. The error bars were obtained by repeating the measurements 10 times.

The focus position can be calibrated in the laboratory against distance to target by imaging a high contrast calibration chart at a range of distances. Fig. 3b shows the distance versus focus position relation for PRISMS where the distance to the target was measured with a Leica Disto D3 laser ranger (typical accuracy 1.0 mm for distances up to 100 m). The accuracy of this calibration can be improved using a more precise distance measurement device. Once calibrated, the relation can be used in the field to determine distances using just the spectral imaging system.

The uncertainties in distance determination using this method is shown in Fig. 3c for a low contrast mock wall painting target (painted in one colour without any features other than the intrinsic surface texture). The distance errors are smallest at short distances but increases steadily with distance. The anomalous large scatter between 11 and 20 m was due to bad 'seeing' (air turbulence and temperature gradient) because the measurements were conducted along a corridor that was divided into 3 sections and the 11–20 m range intersects with other corridors leading to increased air turbulence. The distance accuracy is ultimately limited by the signal-to-noise ratio (SNR) of the images and air turbulence. It is important to note that the distance accuracy can be much better than the depth of field, in the same way that position accuracy can be much better than the imaging resolution if the SNR is high. There is a trade-off between distance accuracy and speed of imaging.

Distances to the centre of each field of view (FOV: $0.31^\circ \times 0.23^\circ$) is determined as the spectral images are taken without any additional measurements. This gives a coarse global shape measurement as a by-product of spectral imaging without reducing the speed of image scanning. For example, when imaging a mock wall painting target at a distance of ~ 5 m, we expect a distance measurement, at millimetre accuracy, every ~ 2 cm across the wall; the relative position accuracy in the transverse direction corresponds to the image pixel size of ~ 20 μm at this distance. Such accuracy is comparable to laser scanning (Amann et al., 2001; Fryer

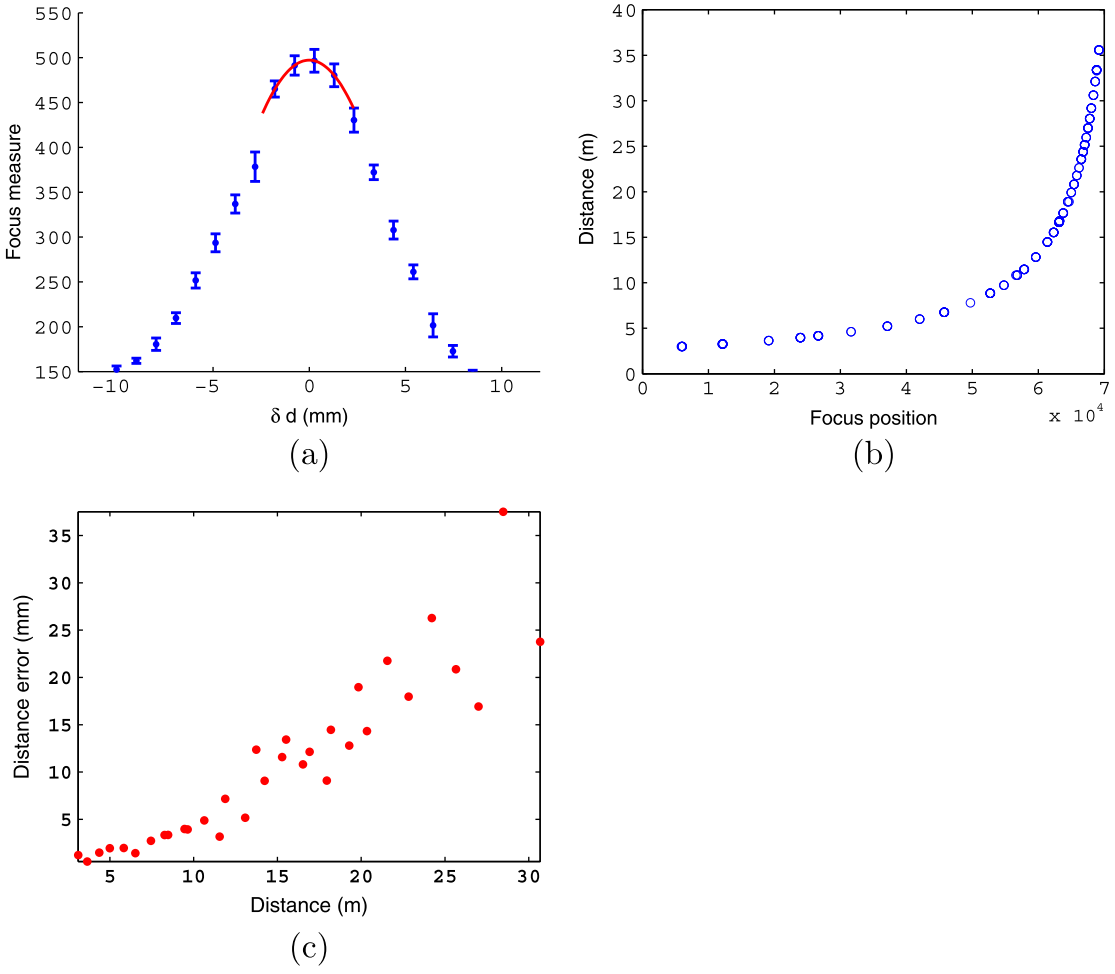

Fig. 3. (a) An example of focus measure using the EoG metric versus relative distance centred around ~7 m (the data points are in blue and the red curve is the Gaussian fit); (b) calibration curve for distance to target versus focus position relation; (c) Distance error (rms) versus distance to target in the worst case scenario of imaging a featureless mock wall painting tile. (For interpretation of the references to colour in this figure legend, the reader is referred to the web version of this article.)

et al., 2005). The advantage of the current method is that the distance measurements do not require additional instruments nor extra capture and processing time. There is also no need to co-register the 3D spatial and spectral data as they are taken with the same imaging instrument at the same time.

If texture mapping is required at smaller spatial scales, individual images can be saved as the system is focusing which allows focus positions for sub-regions of each FOV to be determined instead of the central ROI. This will slow down the data capture as extra time is needed for processing each sub-region.

3.3. Radiometry

In conventional imaging in a lab, the radiometric calibration involves (i) a flatfield calibration to remove the non-uniform illumination and the pixel-to-pixel gain variation of the detector by imaging a matte white card at the position of the target and (ii) an absolute reflectance calibration by imaging a white standard of known reflectance at the same position as the target. In remote imaging, it is not possible to place a white card or white standard at each target position. Instead the radiometric calibration will be carried out in the lab by measuring a Spectralon white standard at different distances and angles relative to the optical axis of the imaging system.

The illumination is designed to give a uniform illumination across the 10° beam width and the light is placed next to the camera with its optical axis at an angle of 5° to the camera optical axis such that over the telescope focusing range (d>3 m), the illumination beam always overlaps the entire FOV of the camera (see Fig. 4a). The FOV of the camera is illuminated by different parts of the light beam at different target distances. An inverse square law, relating the intensity of light reflected back from a white standard and its distance from the light, is expected if the light beam is uniform in cross-section. Fig. 4b shows that the measured back reflected intensity is consistent with an inverse square law over the measured distance range between 4 m and 12 m. The data deviates from the inverse square law at distances below 4 m. Therefore, one measurement of a white standard at a given distance in the field can be used to calibrate all measurements at different distances.

The configuration of the lighting and imaging system and the synchronous motions of the two implies that reflectance is measured in near retro-reflection geometry with the lighting axis always at an angle of $\sim 5^\circ$ from the imaging axis.

3.4. Spectrometry

Spectral calibration can be carried out by imaging a Spectralon white standard at a convenient distance at the start and end of the imaging run. Spectrum of the light source was found to stay constant within <1% over 13 days.

Fig. 5 shows the spectra of various colour patches from a mini-Macbeth chart measured by PRISMS and an Ocean Optics HR2000 fibre optic spectrometer, with both measurements conducted at the standard 45°/0° configuration for illumination and collection of light. The measurements agree within the error margins.

4. Remote imaging of cave paintings at a UNESCO site

The Mogao caves near Dunhuang at the edge of the Gobi desert is a Buddhist temple site with a history that extends over 1000 years from the 4th century to the 15th century. There are 735 caves (492 with wall paintings) and 45,000 square metres of wall paintings at the site, which is an immense resource for the study of the history of art and architecture, religion, science and technology, politics and cultural exchange along the Silk Road. The wall paintings are vulnerable since they are exposed to the elements and recording as much information as possible of the current state of the paintings is both a form of digital preservation in case of future lose of the paintings as well as a means for scientific examination to inform conservation and art historical studies.

4.1. Large scale 3D spectral imaging

Fig. 1b shows the setup of PRISMS in one of the caves at the Mogao site.

Fig. 6a shows the ceiling of cave 55 at the Mogao site illuminated by the lighting system of PRISMS. Cave 55 is a Buddhist cave temple constructed in the 10th–11th century. Fig. 6b shows a high resolution image captured at the ground level of a patch of the ceiling 11 m away that gives a detailed image of clusters of green pigment particles. The colour image was derived from the multispectral images assuming a standard D65 daylight illumination and the CIE 1931 2° standard observer colour matching functions (CIE Colorimetry, 2004; McLaren, 1976). The individual colour images are automatically stitched into a seamless mosaic using a cross-correlation routine that returns a maximum when the overlapped regions between the images are matched (Fig. 6c). The imaging system is designed such that the images are captured from a single view point. This has the advantage of avoiding parallax effects, however, it also means that the imaging geometry is not constant relative to the target. This is not necessarily a problem, since the geometries of the measurements are known, the reflectance measurements are accurate with respect to the known geometries. In particular, it presents the paintings in the colour as they would be viewed by a person standing at the position of the camera. Fig. 7a shows the change in back-reflected light

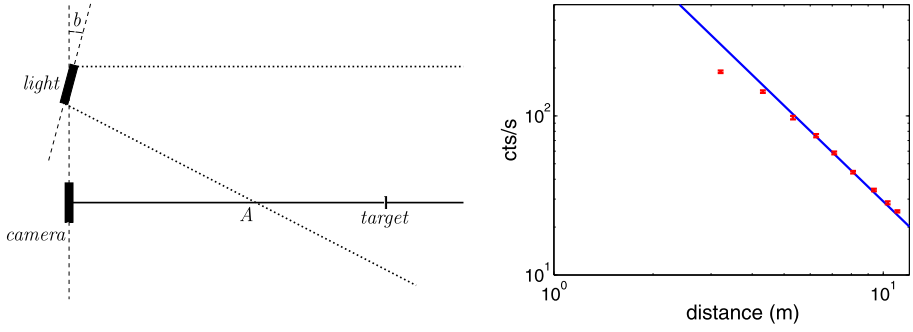

Fig. 4. (a) A schematic diagram of the relative geometry between the light beam, the camera system and the target to determine the relation between the intensity of the light reflected versus the distance. The point *A* is at 2.3 m and the angle between the light and the camera axes is 5°. (b) Intensity of light reflected from a Spectralon white standard as a function of distance. The straight line corresponds to an inverse square law ($I \propto d^{-2}$).

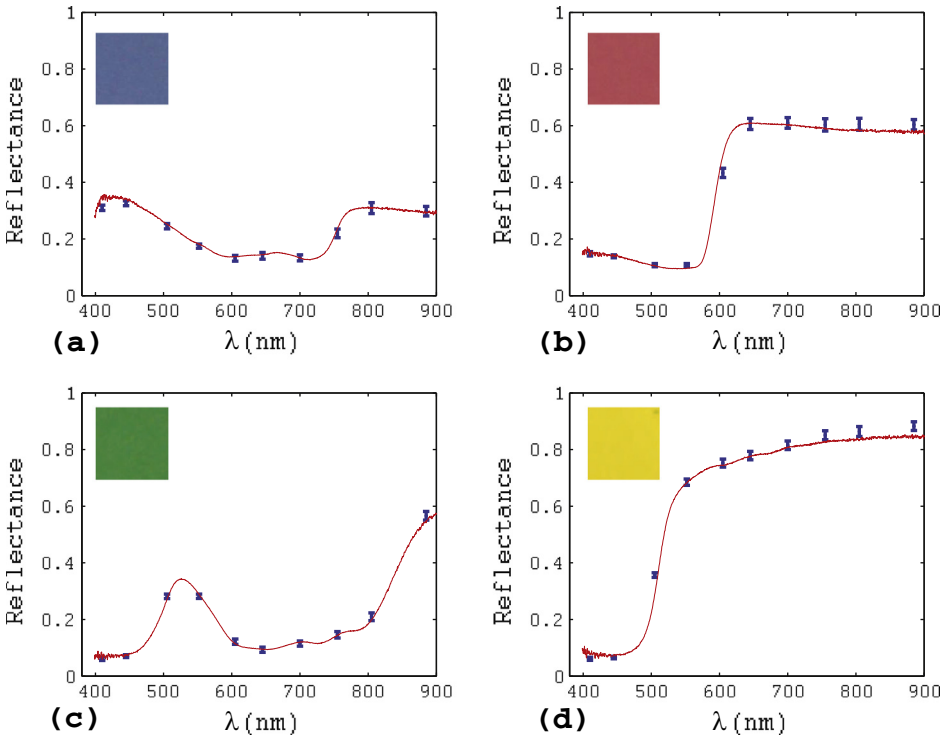

Fig. 5. Macbeth colour patches 8, 10, 14, 15: PRISMS measured spectra compared with spectrometer measured spectra at 0°/45° geometry (solid curve).

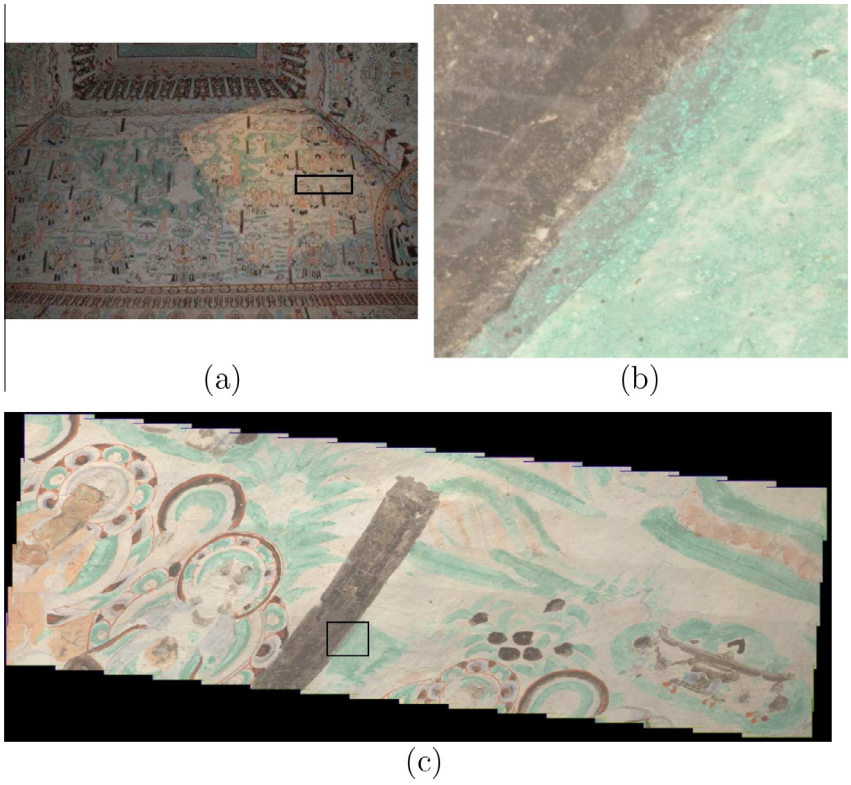

Fig. 6. (a) View of the east ceiling of Mogao cave 55 from the position of the imaging system at a distance of ~11 m using a normal camera; (b) high resolution colour image of the ceiling (corresponding to the area in (c) marked with a black square) derived from PRISMS images showing the green pigment particle clusters (image size corresponds to 3×2.4 cm^2 on the ceiling); (c) an automatically mosaiced image of part of the ceiling (area in (a) marked with a black square). (For interpretation of the references to colour in this figure legend, the reader is referred to the web version of this article.)

intensity as a function of the angle between the normal of the target surface and the optical axis of the imaging system for a Spectralon white standard. In some caves, there are statues in the middle which can block the view to a wall from the camera. This will then necessitate imaging from another view point. Alignment of scans from different view points will need to be

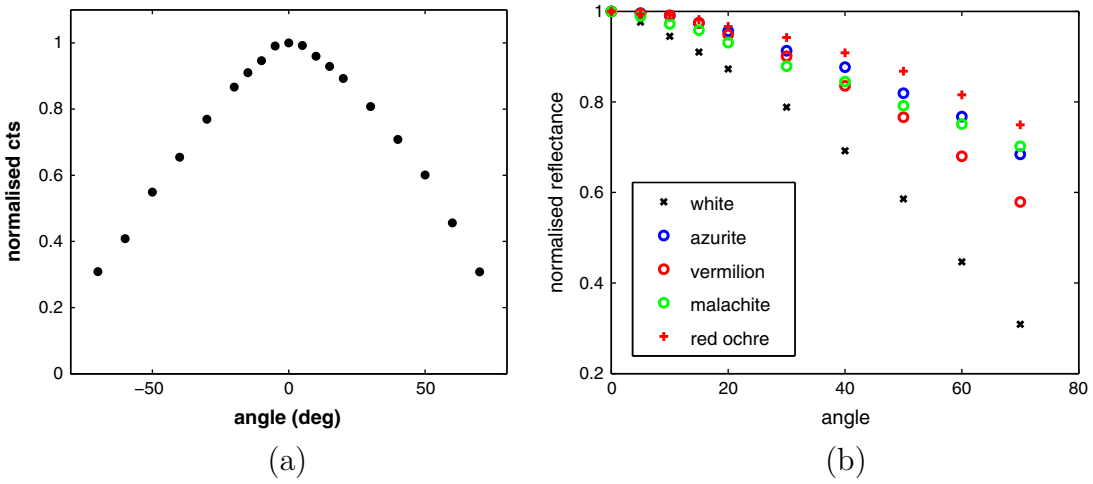

Fig. 7. (a) Normalised intensity measured through the 880 nm filter as a function of angle between the normal of the target surface and the optical axis of the camera at a distance of ~7 m for the matte Spectralon white standard; (b) a comparison of the angular dependence of the reflected intensity of light at 880 nm for different colour patches on a mock wall painting tile (picture shown in Fig. 10a) and the Spectralon white standard. (For interpretation of the references to colour in this figure legend, the reader is referred to the web version of this article.)

implemented in the future by using common areas scanned in both view points as references.

All the image processing are performed using the VIPS library (Cupitt and Martinez, 1996). The capturing and mosaicing process transforms and projects the paintings onto a plane tangential to a sphere centred at the camera with a radius equal to the distance between the camera and the part of the painting that is used as the reference image in the mosaicing process. The mosaiced image can then be projected back onto the 3D surface of the painting measured by the imaging process as detailed in Section 3.2 to produce a virtual 3D reconstruction in colour or any of the spectral bands, thus representing the 3D topography together with the multispectral images and the derived colour image. Such a visualisation makes it a convenient tool for conservators.

4.2. Revealing detailed drawings and faded writings

The date of construction of Mogao cave 465 is still under debate amongst art historians. The range of dates vary between the 9th and the 13th century. Any extra information in terms of drawing styles or hidden writings would help to inform historical studies. Fig. 8 shows that the drawings which are not seen in the colour image are clearly revealed in the near infrared image at 880 nm.

Fig. 9 shows the images of a region on the western parts of the ceiling obtained with PRISMS from a distance of 17 m. No writing can be seen in the colour image or the near infrared image (880 nm). However, a difference image between 880 nm and 550 nm revealed the Sanskrit writing even though no writing can be seen in either of the two images. This demonstrates the powers of multispectral imaging in revealing faded writing. As the spectra of the writing has a greater difference in the two spectral bands than the background, the difference image enhances the writing while removing the common background.

4.3. Pigment identification

A mock wall painting tile was made up in a similar manner as those found on the cave walls. Five most common pigments mixed in animal glue were painted out on a tile plastered with clay and straw and prepared with a traditional white ground layer (Fig. 10). As discussed in Section 4.1, the intensity of the reflected light depends on the angle of incidence (see Fig. 7a) and the surface texture of the target. It was found that this angular dependence is much weaker for the wall painting tile compared with a matte Spectralon white standard (Fig. 7b). Fig. 10 shows the spectral reflectance of the 5 types of paint on the wall painting tile measured at various angles of incidence using the measurements of the white standard at the same angle as a reference. While the intensities change as a function of the angle, the spectral shapes are independent of the angles and consistent with spectrometer

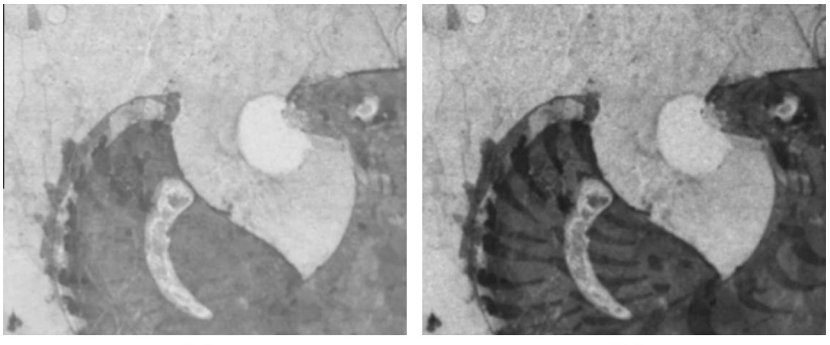

Fig. 8. Mogao cave 465 top of the east side of the south wall (~3.5 m above ground, imaged from a distance of ~8 m) showing the drawing details in the 880 nm near infrared channel (b) which were not seen in the colour image (a).

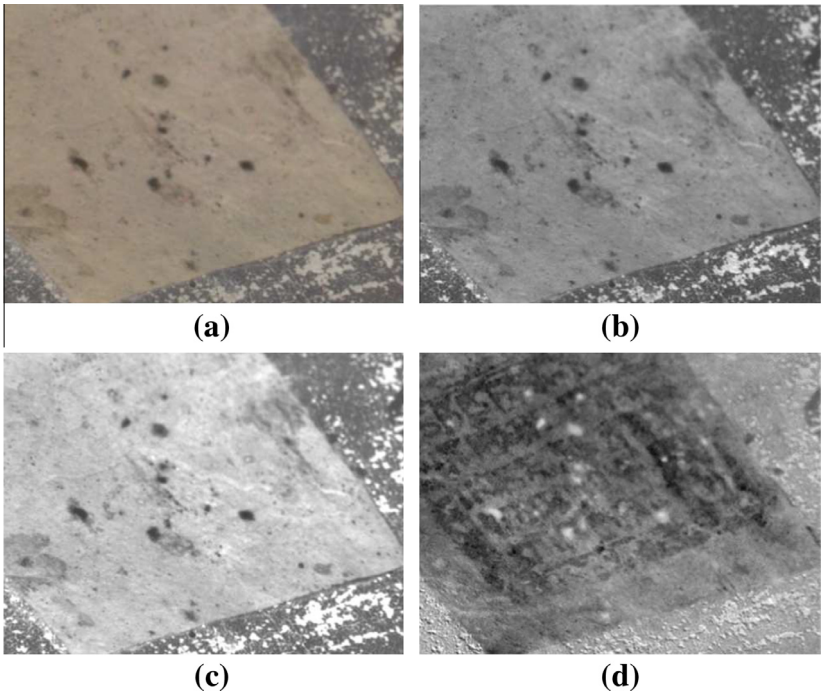

Fig. 9. Revealing Sanskrit writing in Mogao cave 465: (a) Image of writing on the western ceiling in colour; (b) image at 550 nm; (c) image at 880 nm; (d) difference image between 550 nm and 880 nm. (For interpretation of the references to colour in this figure legend, the reader is referred to the web version of this article.)

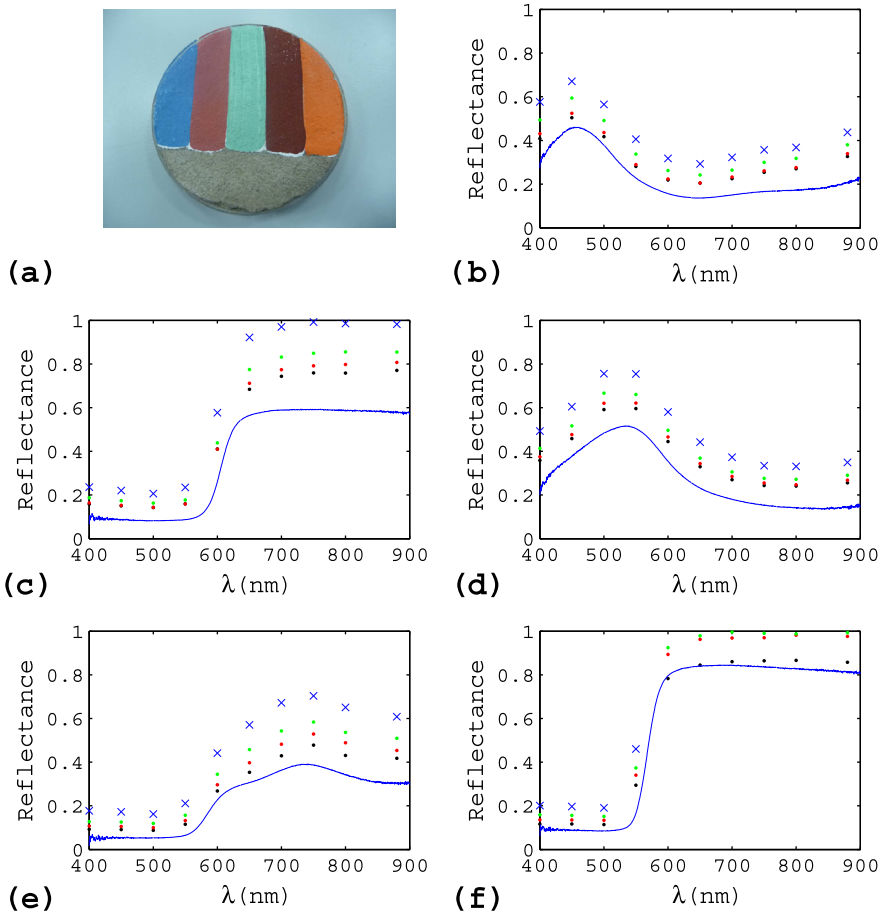

Fig. 10. (a) Mock wall painting tile with colour patches of the most common paint found in Mogao caves from left to right: azurite, vermilion, malachite, red ochre and red lead in animal glue. (b–f) PRISMS measured spectra from a distance of 8 m at 0° (black dot), 30° (red dot), 45° (green dot) and 60° (blue cross) compared with spectrometer measured spectra at 45°/45° (blue curve) for azurite (b), vermilion (c), malachite (d), red ochre (e), red lead (f). (For interpretation of the references to colour in this figure legend, the reader is referred to the web version of this article.)

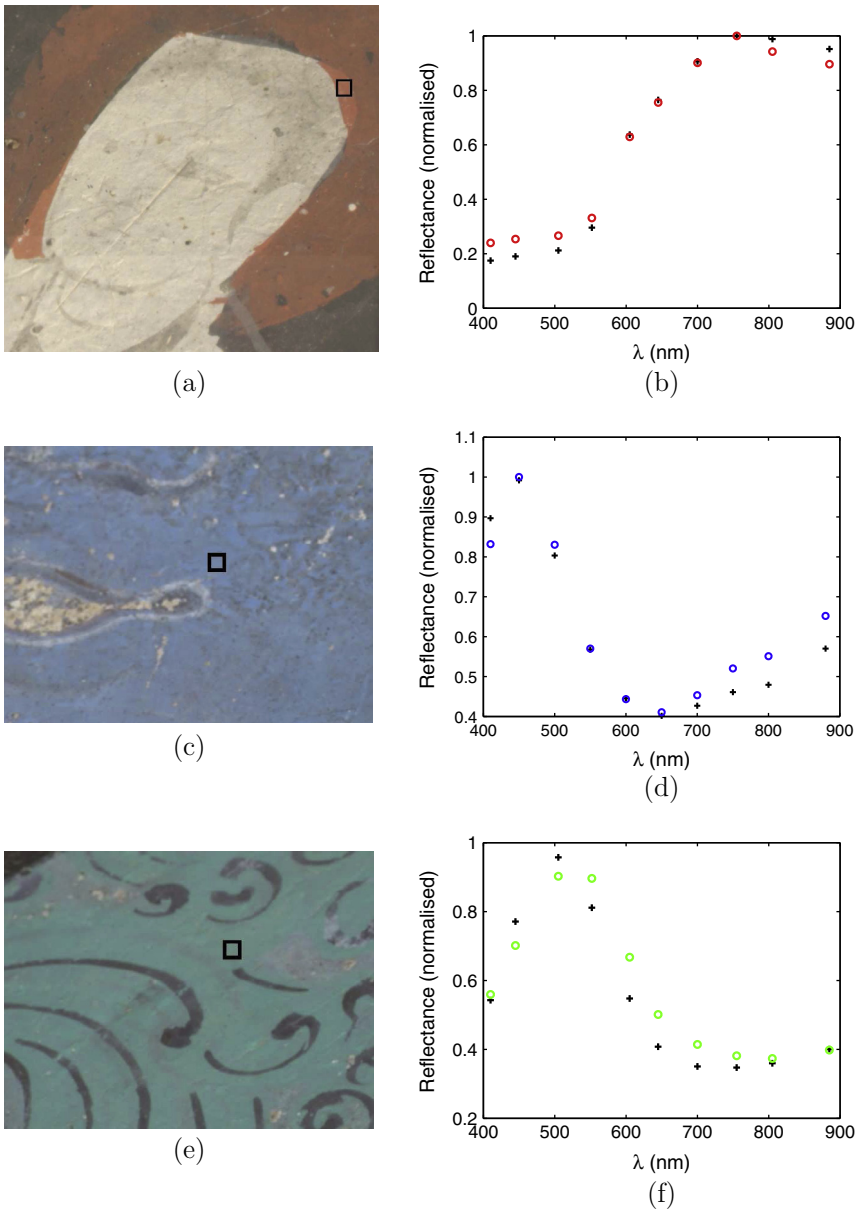

Fig. 11. Pigment identification in Mogao caves 55 and 465: (a) and (b) cave 55 red paint identified with red ochre; (c) and (d) cave 465 blue paint identified with azurite; (e) and (f) cave 465 green paint identified with malachite. The circles are the normalised PRISMS measured reference spectra from the mock wall painting tile and the crosses are the normalised PRISMS measured spectra from the cave wall paintings. (For interpretation of the references to colour in this figure legend, the reader is referred to the web version of this article.)

measured spectra. Therefore pigment identification will not be affected by the angles of incidence.

Fig. 11 shows some examples of pigment identification in two of the caves. The red paint is unambiguously identified with red ochre. In the case of the blue pigment, areas with a similar spectral shape at a more accessible height were examined with a portable Niton X-ray Fluorescence (XRF) spectrometer and found to contain copper which is consistent with the identification of azurite. XRF gives elemental information but spectral reflectance in the visible/NIR gives the characteristics of the compound. Similarly, for the green pigment, XRF found the presence of Cu for an area with similar spectral reflectance which is also consistent with the pigment malachite. However, it is known that at Mogao another copper containing green pigment atacamite is also used. Unfortunately, malachite and atacamite have very similar spectral shape in the 400–900 nm range. Spectral imaging at longer wavelengths or Raman spectroscopy could potentially distinguish between the two.

5. Conclusions

The versatile remote spectral imaging system, PRISMS, is capable of high resolution imaging at a resolution of 8.2 μrad (or 1.7″) which translates to 80 μm at a distance of 10 m. It is the first spectral imaging system to simultaneously measure spectral reflectance and 3D shape of the imaging target without additional distance measurement devices. This eliminates the complexity and cost of multiple instruments and the need for extra processing in order to co-register 3D data and spectral images. The on-line distance measurement is a by-product of spectral imaging as passive focusing is used to focus the images. Distance accuracy of a few mm were achieved on wall painting targets at distances of 10 m.

On site remote imaging with PRISMS at a UNESCO world heritage site, Mogao caves, has demonstrated a broad range of applications of spectral imaging in art conservation, history and archaeology. It has found faded Sanskrit writings on the ceilings of cave 465 that were not visible in any of the spectral bands or colour images, revealed invisible drawings and identified pigments. PRISMS records the 3D shape, spectral reflectance and therefore colour images remotely from one position on the ground making it convenient for large scale recording of a range of quantitative data as well as detailed examination of specific parts of a cave painting for scientific and art historical studies. It would be interesting in the future to compare the topographic measurements obtained with PRISMS with a conventional laser scan in the same cave.

Acknowledgements

Funding from the UK Engineering and Physical Science Research Council (EP/E016227/1), Chinese Ministry of Science and Technology 973 Program (2012CB720906) are gratefully acknowledged. We would like to thank Simon Godber, David Parker and Mike Newton of Nottingham Trent University for technical assistance, Zhang Huabin, Mao Jiaming, Chai Bolong and other colleagues from Dunhuang Academy for assistance with on site data collection, Cui Qiang and Yu Zongren for the XRF data. Dunhuang Academy is in charge of the conservation and management of the Mogao caves.

References

Amann, M., Bosch, T., Lescure, M., Myllylä, R., Rioux, M., 2001. Laser ranging: a critical review of usual techniques for distance measurement. Opt. Eng. 40 (1), 10–19.

Barazzetti, L., Remondino, R., Scaioni, M., Brutto, M., Rizzi, A., Brumana, R., 2010. Geometric and radiometric analysis of paintings in international archives of photogrammetry. In: Remote Sensing and Spatial Information Science, Part 5, Commission V Symposium, vol. XXXVIII, pp. 62–67.

Baronti, S., Casini, A., Lotti, F., Porcinai, S., 1998. Multispectral imaging system for the mapping of pigments in works of art by use of principal-component analysis. Appl. Opt. 37, 1299–1309.

Brusco, N., Capeleto, S., Fedel, M., Paviotti, A., Poletto, L., Cortelazzo, G., Tondello, G., 2006. A system for 3D modeling frescoed historical buildings with multispectral texture information. Mach. Vis. Appl. 17, 373–393.

Burmester, A., Cupitt, J., Derrien, H., Dessipris, N., Hamber, A., Martinez, K., Müller, M., Saunders, D., 1993. The examination of paintings by digital image analysis. In: 3rd International Conference on Non Destructive Testing, Microanalytical Methods and Environmental Evaluation for Study and Conservation of Works of Art, Rome 1993, pp. 210–214.

Casini, A., Lotti, F., Picollo, M., Stefani, L., Buzzegoli, E., 1999. Image spectroscopy mapping technique for noninvasive analysis of paintings. Stud. Conserv. 44, 39–48.

CIE Colorimetry, 2004. 3rd Ed. CIE Publication 015:2004. Central Bureau of the CIE, Vienna.

Cupitt, J., Martinez, K., 1996. VIPS: an image processing system for large images. Proc. SPIE 1663, 19–28.

Fischer, C., Kakoulli, J., 2006. Multispectral and hyperspectral imaging technologies in conservation: current research and potential applications. Rev. Conserv. 3–16 (2006).

Fryer, J., Chandler, J.H., El-Hakim, S., 2005. Recording and modelling an aboriginal cave painting: with or without laser scanning? In: El-Hakim, Sabry, Remondino, Fabio, Gonzo, Lorenzo (Eds.), ISPRS Archives, WG V/4 3D-ARCH 2005: Virtual Reconstruction and Visualization of Complex Architectures 22–24 August, 2005, Vol. XXXVI-5/W17. Mestre-Venice, Italy.

Goetz, A., Vane, G., Solomon, J., Rock, B., 1985. Imaging spectrometry for earth remote sensing. Science 228, 1147–1153.

Huang, W., Jing, Z., 2007. Evaluation of focus measures in multi-focus image fusion. Patt. Recog. Lett. 28, 493–500.

Kubik, M., 2007. Hyperspectral imaging: a new technique for the non-invasive study of artworks. In: 2007 Physical Techniques in the Study of Art, Archaeology and Cultural Heritage, vol. II. Amsterdam, pp. 199–255.

Liang, H., 2012. Advances in multispectral and hyperspectral imaging for archaeology and art conservation. Appl. Phys. A 106, 309–323.

Liang, H., Keita, K., Vajzovic, T., 2007. PRISMS: a portable multispectral imaging system for remote in situ examination of wall paintings. In: Proceedings of the SPIE 6618, 661815.

Liang, H., Keita, K., Pannell, C., Ward, J., 2010. A SWIR hyperspectral imaging system for art history and art conservation. In: IX CONGRESO NACIONAL DEL COLOR. Alicante, Spain, pp. 189–192.

Liang, H., Lange, R., Peric, B., Spring, M., 2013. Optimum spectral window for imaging of art with optical coherence tomography. Appl. Phys. B 111 (4), 589–602.

Liang, H., Saunders, D., Cupitt, J., 2005. A new multispectral imaging system for examining paintings. J. Imag. Sci. Technol. 49 (6), 551–562.

Macdonald, L., 2006. A robotic system for digital photography. In: Proceedings of the SPIE 6069, 60690I.

Mara, H., Breuckmann, B., Lang-Auinger, C., 2009. Multi-spectral high-resolution 3D-acquisition for rapid archaeological documentation and analysis. In: Proceedings of 17th European Signal Processing Conference (EUSIPCO'09). Glasgow, UK, pp. 1205–1209.

Martinez, K., Cupitt, J., Saunders, D., 1993. High resolution colorimetric imaging of paintings. In: Proceedings of the SPIE 1901, pp. 25–36.

McLaren, K., 1976. The development of the CIE 1976 (L^* a^* b^*) uniform colour space and colour-difference formula. J. Soc. Dyers Colour. 92, 338–341.

Nayar, S.K., Nakagawa, Y., 1994. Shape from focus. IEEE Trans. Pattern Anal. Mach. Intell. 16 (8), 824–831.

van Asperen de Boer, J.R.J., 1968. Infrared reflectography: a method for the examination of paintings. Appl. Opt. 7, 1711–1714.

Wallach, H., 2004. High resolution photography at the Dunhuang Grottoes. In: Conservation of Ancient Sites on the Silk Road – Proceedings of the Second International Conference on the Conservation of Grotto Sites. Dunhuang, China, pp. 259–261.